

Electron capture by slow Al^{q+} ions colliding with hydrogen

R. A. Phaneuf

Physics Division, Oak Ridge National Laboratory, Oak Ridge, Tennessee 37831

M. Kimura,* H. Sato,† and R. E. Olson

Physics Department, University of Missouri—Rolla, Rolla, Missouri 65401

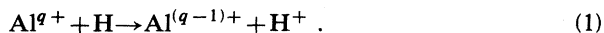
(Received 14 January 1985)

Total electron-capture cross sections have been measured for collisions of Al^{q+} ($q=2-10$) with H and H_2 in the 20–120-eV/amu energy range. The general trend of the cross sections for both H and H_2 is an approximately linear increase with ionic charge state. The $\text{Al}^{2+} + \text{H}$ and $\text{Al}^{3+} + \text{H}$ systems were investigated theoretically using the molecular-orbital method with a pseudopotential to represent the Al^{3+} ion core. Coupled-channel calculations realize good agreement with experiment. An anomalously small cross section for $\text{Al}^{2+} + \text{H}$ is attributed to the fact that of the $^1\Sigma$ and $^3\Sigma$ entrance channels, only the $^1\Sigma$ molecular state contributes to the cross section.

I. INTRODUCTION

The development of a laser-produced-plasma ion source¹ has made it convenient to study low-energy electron-capture collisions involving highly-stripped metal ions, and total cross sections² have recently been reported for Fe^{q+} ions colliding with H and H_2 . Such collisions are of interest to the modeling of ion transport in fusion reactors since the container walls and plasma-limiter surfaces are the source of most of the impurity ions. Correspondingly, collisions involving Al^{q+} ions are of special interest to some small-scale test reactors such as the ELMO Bumpy Torus (EBT) at Oak Ridge, which has an aluminum container.

In this paper we present a combined experimental-theoretical study of the low-energy electron-capture reaction



Cross sections for charge states q between 2 and 10 have been measured for both H and H_2 gas targets in the energy range of 20 to 120 eV/amu. Coupled-channel calculations have been made for $q=2$ and 3 at energies from 20 to 10000 eV/amu. Good agreement is obtained with the experimental measurements for H, giving credence to the theoretical procedure. Brief descriptions of the methods and results are given in the following sections.

II. EXPERIMENTAL

The apparatus and time-of-flight technique used for electron-capture cross-section measurements have been described recently.^{1,3} A 2-J, 60-ns pulse of CO_2 -laser radiation is focused in vacuum onto an aluminum metal target. A series of apertures collimate a beam from the expanding plasma which enters an electrostatic analyzer. A beam emerges from the analyzer with selected energy per charge, passes through a calibrated thermal-dissociation atomic hydrogen target, is once more charge analyzed by electrostatic deceleration, and detected by an electron mul-

tiplier. Charge separation is effected by time-of-flight analysis. Electron-capture cross sections are deduced by measuring the variation with target thickness of the net fraction of ions which capture an electron in the hydrogen target. The atomic and molecular hydrogen target thicknesses and dissociation fraction (0.87 ± 0.03) were determined in an auxiliary experiment using a probe beam of 20-keV protons.⁴

III. THEORETICAL

The details of the theoretical treatment have been presented,^{5,6} so we will only outline the basic techniques and the specific information needed for the $\text{Al}^{2+} + \text{H}$ and $\text{Al}^{3+} + \text{H}$ calculations. For the collision energy range of interest in this work, we have employed the molecular-orbital expansion method with electron translation factors appropriate for one- and two-electron systems. The molecular energies and wave functions were calculated using linear combinations of Slater determinants. Slater-type orbitals were employed.

For the calculations, the $\text{Al}^{3+}(1s^2 2s^2 2p^6)$ ion core was represented by an l -dependent pseudopotential of the form⁷

$$V(r) = \sum_{l,m} V_l(r) |Y_{lm}\rangle \langle Y_{lm}| , \quad (2)$$

$$V_l(r) = A_l \exp(-\xi_l r^2) - \frac{\alpha_d}{2(r^2 + d^2)^2} - \frac{\alpha_q}{2(r^2 + d^2)^3} - \frac{3}{r} . \quad (3)$$

The dipole and quadrupole polarizabilities were obtained from a review by Dalgarno.⁸ The other parameters were determined from spectroscopic data and are given in Table I. The orbital exponents for the basis set are given in Table II. Except for the Al 3s orbital exponents which were obtained from Clementi and Roetti,⁹ the Al values were obtained by optimizing for the lowest energy of their

TABLE I. Al^{3+} pseudopotential parameters (in atomic units).

A_0	+ 20.665 625
A_1	+ 8.925 184 1
A_2	- 4.676 947 8
ξ_0	+ 2.167 684 7
ξ_1	+ 1.584 287 4
ξ_2	+ 2.576 184 3
d	0.600 5
α_d	0.357
α_q	0.237

respective electronic levels. The H basis set is exact through $n = 2$, with a $2p$ orbital exponent of 1.0 added to improve the accuracy of the dipole polarizability of H. The calculated $\text{Al}^{2+}(3s)$, $\text{Al}^{2+}(3p)$, and $\text{Al}^{2+}(3d)$ levels reproduce the spectroscopic ionization energies to 0.025, 0.043, and 0.070 eV, respectively. Because of the added complication of electron correlation, the $\text{Al}^+(3s^2^1S)$ and $\text{Al}^+(3s3p^1P)$ levels only reproduce the spectroscopic values to within 0.013 and 0.191 eV, respectively.

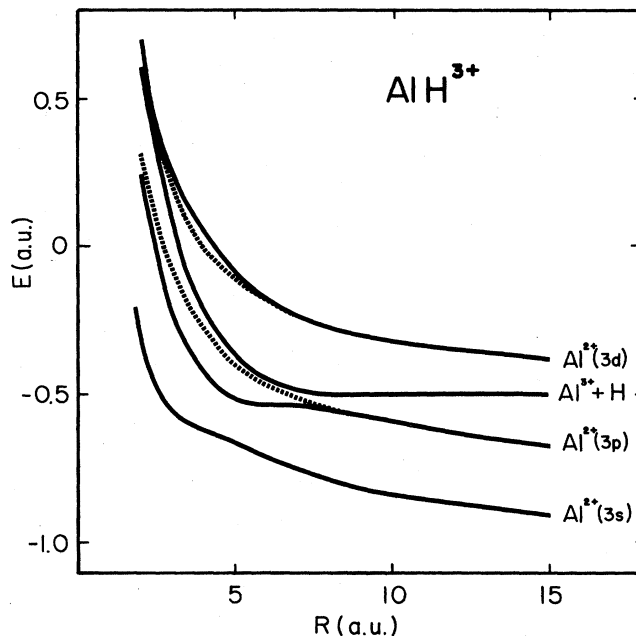
The molecular-orbital calculations for the $^2\Sigma$ and $^2\Pi$ states of AlH^{3+} are straightforward one-electron configuration interaction computations. The interaction energies are presented in Fig. 1. Even before starting the scattering calculations, it is apparent the dominant interaction will be at $R \approx 6a_0$ and lead to electron capture to the $\text{Al}^{2+}(3p) + \text{H}^+$ state.

A complete two-electron configuration interaction calculation (all possible single- and double-electron excitations—127 configurations) was performed for the molecular structure of the $^1\Sigma$ states of AlH^{2+} , see Fig. 2. The $^1\Pi$ molecular states were not evaluated since their effect on the total cross section will be negligible. The triplet states also were not evaluated since the lowest-lying electron-capture channel leads to $\text{Al}^+(3s3p^3S) + \text{H}^+$, which is endothermic to the $\text{Al}^{2+} + \text{H}$ entrance channel. Hence, no strong curve-crossing interactions will be available to populate triplet levels.

For both systems, the scattering calculations were made using the perturbed-stationary-state close-coupling method with straight-line trajectories. Electron translation factors were incorporated in the close-coupling equation by retaining coupling terms to first order in the collision velocity.^{5,6} The inclusion of electron translation

TABLE II. Orbital exponents of the Slater-type-orbital basis functions.

	Al		H	
3s	4.703		1s	2.00
	2.962			1.00
	1.773			0.50
	1.093			
3p	1.944		2s	0.50
	1.534		2p	1.00
	0.910			0.50
3d	1.069			

FIG. 1. Interaction energies for the $^2\Sigma$ (solid lines) and $^2\Pi$ (dashed lines) for the low-lying molecular states of AlH^{3+} .

factors allows the coupling terms to dissociate properly, thus removing fictitious long-range behavior.

The scattering calculations on the AlH^{3+} system included six molecular states composed of $^2\Sigma$ and $^2\Pi$ states that dissociate to the $\text{Al}^{3+} + \text{H}$ initial channel, and the $\text{Al}^{2+}(3s)$, $\text{Al}^{2+}(3p)$, and $\text{Al}^{2+}(3d)$ electron-capture channels. All possible combinations of the radial and rotational coupling terms were included in the calculations. For the AlH^{2+} system, the three $^1\Sigma$ molecular states dissociating to $\text{Al}^{2+}(3s)$, $\text{Al}^+(3s^2)$, $\text{Al}^+(3s3p)$ were included along with all combinations of the radial coupling terms.

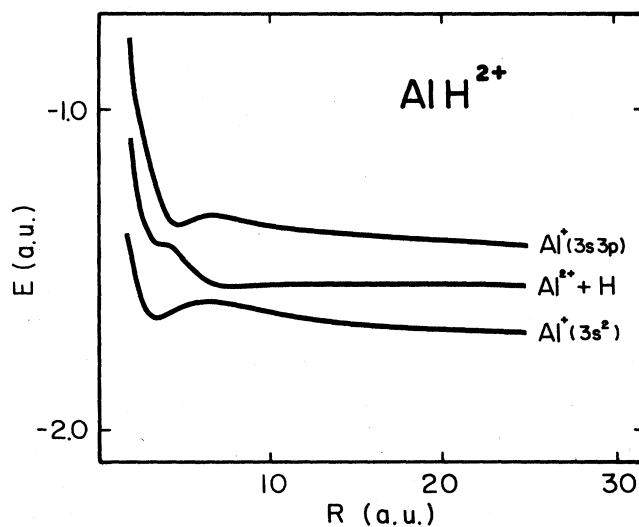
FIG. 2. Interaction energies for the three-lowest $^1\Sigma$ molecular states of AlH^{2+} .

TABLE III. Total experimental electron-capture cross sections for Al ions colliding with H and H₂.

q	Energy (eV/amu)	Relative Velocity (10^7 cm/s)	$\sigma_{q,q-1}(\text{H})$ (present data) ^a (10^{-16} cm ²)	$\sigma_{q,q-1}(\text{H}_2)$ (present data) ^a (10^{-16} cm ²)	$\sigma_{q,q-1}(\text{H}_2)$ (Schrey and Huber) (10^{-16} cm ²)
2	23.9	0.68	< 1	13.6±3.2(4.3)	
2	51.8	1.00			13
3	35.9	0.83	16.3±3.2(4.8)	40.1±2.5(8.4)	
3	55.6	1.03			52
4	47.8	0.96	39.1±4.4(9.2)	42.0±2.9(8.4)	
4	118.5	1.51			34
5	59.8	1.07	40.8±3.2(8.6)	56.5±2.7(10.4)	
5	92.6	1.33			75
6	71.1	1.18	40.8±4.3(8.7)	54.8±2.3(9.4)	
7	83.7	1.27	78.2±4.3(14.5)	63.3±2.2(10.2)	
8	95.6	1.36	73.6±3.6(13.0)	59.3±0.9(8.9)	
9	107.6	1.44	82.2±3.9(14.6)	59.5±2.6(10.0)	
10	119.5	1.52	85.6±8.4(15.9)	82.8±5.6(12.7)	

^aQuoted uncertainties are, respectively, the reproducibility at one standard deviation, and (in parentheses) the total estimated experimental uncertainty at good-confidence level.

IV. RESULTS AND DISCUSSIONS

The experimental cross sections for $\text{Al}^{q+} + \text{H}$ and $\text{Al}^{q+} + \text{H}_2$ collisions are given in Table III along with the random and estimated total experimental uncertainties. Experimental data of Schrey and Huber¹⁰ for $\text{Al}^{q+} + \text{H}_2$ at similar collision velocities are also tabulated for $q=2-5$ for comparison. Systematic uncertainties are essentially as outlined in Ref. 1, with the exception that those uncertainties associated with relative ion-detection efficiency are progressively lower for the higher q ions of this investigation, since the relative change in q between primary and product ions decreases. For $\text{Al}^{q+} + \text{H}$, the estimated absolute systematic uncertainty at good-confidence level varies from $\pm 32\%$ for $q=2$ to $\pm 14\%$ for $q=10$.

The variation with charge q of the total capture cross sections for $\text{Al}^{q+} + \text{H}$ collisions is shown in Fig. 3 along with the predictions of the absorbing-sphere model of Olson and Salop¹¹ and the multichannel Landau-Zener theory with rotational coupling of Janev, Belić, and Bransden¹² for fully-stripped ions. The $\text{Al}^{q+} + \text{H}$ data are not all taken at exactly the same collision velocity, but vary from 0.7×10^7 cm/s for Al^{2+} to 1.5×10^7 cm/s for Al^{10+} . These differences are considered to be insignificant, since the velocity dependence is expected to be weak¹¹ in this region, especially for $q > 3$. The $\text{Al}^{q+} + \text{H}$ cross sections increase on the average with ionic charge in an approximately linear fashion with a notable deviation for $q=2$, for which the cross section is found to be extremely small.

The absorbing-sphere model predicts a monotonic increase of the capture cross section with ionic charge in this velocity range, but tends to overestimate present measurements. The multichannel Landau-Zener calculations for fully-stripped ions predict strong oscillations about a general increase with ionic charge due to the discreteness of the multicharged ion energy spectrum and the resonant selectivity of the capture process at a given energy. Such behavior is also predicted by the classical model of

Ryufuku, Sasaki, and Watanabe.¹³ The data for partially-stripped $\text{Al}^{q+} + \text{H}$ exhibit a charge scaling which is intermediate between the monotonic rise of the absorbing-sphere model and the strong oscillatory behavior of the Landau-Zener and classical predictions for bare projectile ions. This is to be expected since the presence of ionic core electrons for the partially-stripped Al^{q+} ions removes the l degeneracy which is characteristic of the hydrogenic product-ion states. The product-ion energy-level spectrum remains discrete, but becomes considerably more uniformly distributed in energy as the size of the core increases, and more curve crossings occur in the range of internuclear separations for which capture is

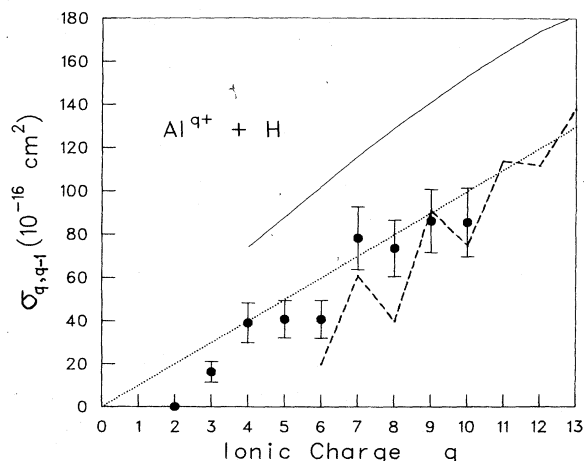


FIG. 3. Experimental total electron-capture cross sections plotted versus ionic charge q for $\text{Al}^{q+} + \text{H}$ at a collision velocity of $4.8 \times 10^6 \sqrt{q}$ cm/s. Flags designate estimated total absolute uncertainty at good-confidence level. The solid curve is the absorbing-sphere model (Ref. 11) and the multichannel Landau-Zener calculation (Ref. 12) is given by the dashed curve. Both refer to a collision velocity of 10^7 cm/s. The dotted line represents the empirical relation, $\sigma = q \times (10^{-15} \text{ cm}^2)$ given in Ref. 2.

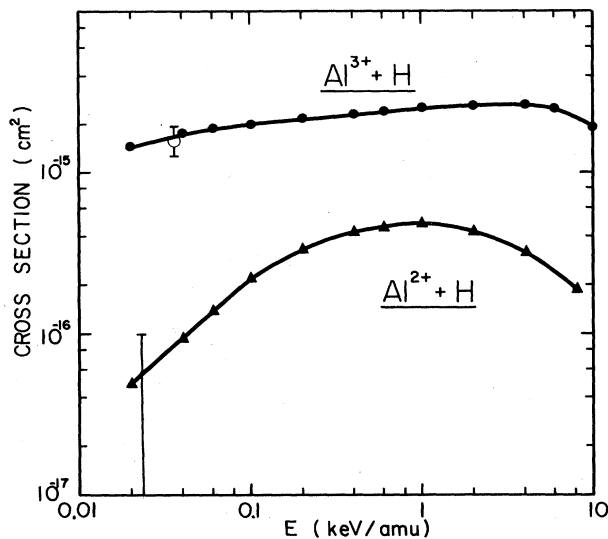


FIG. 4. Coupled-state calculations for the total electron-capture cross sections in $\text{Al}^{3+} + \text{H}$ and $\text{Al}^{2+} + \text{H}$ collisions, solid symbols. The open symbol for $\text{Al}^{3+} + \text{H}$ and flag which represents an experimental upper limit for $\text{Al}^{2+} + \text{H}$ are data obtained using the laser ion source.

most probable. A simple empirical scaling, $\sigma = q \times (10^{-15} \text{ cm}^2)$, was found to give a reasonable average representation for the q scaling of recent $\text{Fe}^{q+} + \text{H}$ measurements, and does comparably well here.

Our coupled-channel calculations for $\text{Al}^{3+} + \text{H}$ and $\text{Al}^{2+} + \text{H}$ collisions are presented in Fig. 4 along with the measurements. The observed electron-capture signal was so weak for $\text{Al}^{2+} + \text{H}$ that we were only able to establish an upper limit of $1 \times 10^{-16} \text{ cm}^2$ for the cross section. For both systems the agreement is considered very satisfactory.

For the $\text{Al}^{3+} + \text{H}$ system, the calculations indicate that the $\text{Al}^{2+}(3p) + \text{H}^+$ electron-capture channel is preferentially populated in the energy range studied. The ratio of the $\text{Al}^{2+}(3p)$ product cross section to the total is almost 100% at energies $E \leq 100 \text{ eV/amu}$, but drops to $\sim 80\%$ at 10 keV/amu. The $\text{Al}^{2+}(3s)$ and $\text{Al}^{2+}(3d)$ share almost

equally the remaining fraction of the total cross section.

For $\text{Al}^{2+} + \text{H}$ collisions, the calculations indicate that the ground-state electron-capture channel, $\text{Al}^+(3s^2) + \text{H}^+$, dominates the products. However, there is an $\sim 25\%$ contribution from the $\text{Al}^+(3s3p) + \text{H}^+$ state at the energies studied. The reason for the anomalously small cross section for $\text{Al}^{2+} + \text{H}$ is not due to an unexpected collision mechanism. The effect is simply due to the statistical weight factor where only 25% of the trajectories follow the $^1\Sigma$ molecular states, while 75% are on the incident $^3\Sigma$ state which does not lead to electron capture. A similar rationale may explain an anomalously small measured cross section¹ for $\text{Fe}^{12+} + \text{H}$, where the incident channels have a higher level of symmetry than possible electron-capture product states.

Landau-Zener calculations have been published for the $\text{Al}^{2+} + \text{H}$ and $\text{Al}^{3+} + \text{H}$ collision systems.¹⁴ These calculations predicted the same dominant product channels as found in our coupled-state calculations. However, the magnitudes of the cross sections are roughly a factor of 2 lower than the present results.

V. SUMMARY

A combined experimental-theoretical study has been made of electron capture in slow collisions of $\text{Al}^{q+} + \text{H}$. The cross sections for the higher charge states, $q \geq 5$, are found to increase on the average in an approximately linear fashion with q . Such behavior is consistent with theoretical models¹¹⁻¹³ and recent experimental data for Fe^{q+} and Xe^{q+} ions.^{2,15} An unusually small cross section for $\text{Al}^{2+} + \text{H}$ collisions is attributed to the statistical weight of the interacting singlet molecular states.

ACKNOWLEDGMENTS

This research was sponsored by the U.S. Department of Energy: The theoretical work was supported by the Division of Applied Plasma Physics of the Office of Fusion Energy and the experimental work by the Division of Chemical Sciences of the Office of Basic Energy Sciences. Oak Ridge National Laboratory is operated by Martin Marietta Energy Systems, Inc., under Contract No. DE-AC05-84OR21400 with the U.S. Department of Energy.

*Present address: Joint Institute for Laboratory Astrophysics, University of Colorado and National Bureau of Standards, Boulder, CO 80309.

†Permanent address: Department of Physics, Ochanomizu University, Otsuka, Bunkyo-ku, Tokyo 112, Japan.

¹R. A. Phaneuf, I. Alvarez, F. W. Meyer, and D. H. Crandall, *Phys. Rev. A* **26**, 1892 (1982).

²R. A. Phaneuf, *Phys. Rev. A* **28**, 1310 (1983).

³R. A. Phaneuf, *IEEE Trans. Nucl. Sci.* **NS-17**, 1182 (1981).

⁴R. A. Phaneuf, F. W. Meyer, and R. H. McKnight, *Phys. Rev. A* **17**, 534 (1978).

⁵M. Kimura, R. E. Olson, and J. Pascale, *Phys. Rev. A* **26**, 3113 (1982).

⁶M. Kimura, H. Sato, and R. E. Olson, *Phys. Rev. A* **28**, 2085 (1983).

⁷J. N. Bardsley, *Case Stud. At. Phys.* **4**, 299 (1974).

⁸A. Dalgarno, *Adv. Phys.* **11**, 281 (1962).

⁹E. Clementi and C. Roetti, *At. Data Nucl. Data Tables* **14**, 77 (1974).

¹⁰H. Schrey and B. A. Huber, *J. Phys. B* **14**, 3197 (1981).

¹¹R. E. Olson and A. Salop, *Phys. Rev. A* **14**, 579 (1976).

¹²R. K. Janev, D. S. Belić, and B. H. Bransden, *Phys. Rev. A* **28**, 1293 (1983).

¹³H. Ryufuku, K. Sasaki, and T. Watanabe, *Phys. Rev. A* **21**, 745 (1980).

¹⁴A. Dalgarno, *Proc. Phys. Soc. London, Sect. A* **67**, 1010 (1954).

¹⁵D. H. Crandall, R. A. Phaneuf, and F. W. Meyer, *Phys. Rev. A* **22**, 379 (1980).